ADVANCED ENGINEERING MATERIALS
www.aem-journal.com

Additive Manufacturing of High-Temperature Preceramic-Derived SiOC Hybrid Functional Ceramics

*Zheng Li, Saurabh Khuje, Abdullah Islam, and Shenqiang Ren**

High-temperature capable materials, metals, and ceramics are attracting significant interest for applications in extreme environmental conditions. Herein, a hybrid metal-reinforced ceramic matrix material consisting of preceramic-derived high-temperature SiOC and copper nanoplates is reported, enabling the manufacturing of high-temperature sensing electronics. The preceramic polymer precursors including polydimethylsiloxane and polydimethylsilane, together with copper nanoplates, are thermally converted into durable copper-reinforced SiOC ceramics. The presence of copper in SiOC ceramics enhances its electrical conductivity, while SiOC suppresses oxygen uptake and acts as a shield for oxidation to achieve high-temperature thermal resistance and negative temperature coefficient at high temperatures. A comprehensive electric and sensing performance, combined with cost-effectiveness and scalability, can facilitate the utilization of hybrid Cu and SiOC composites in high-temperature electronics.

1. Introduction

High-temperature capable materials and electronics have attracted much attention due to their potential use in extreme environments.[1,2] The prospective candidates for high-temperature electronics with high electrical conductivity and antioxidation are limited to a relatively narrow range of noble metals, such as gold (Au),[3] silver (Ag),[4] palladium (Pa),[5] or platinum (Pt).[6] However, these precious metallic materials have relatively low softening and/or melting points compared to that of high-temperature ceramics, making it challenging to manufacture high-temperature robust electronics. The second approach is to optimize the conductor components by alloying (e.g., CuNi, CuAg) or surface modification (e.g., graphene, boron nitride) to resist extreme high temperatures.[7–10] Nevertheless, it suffers from a drastic decrease in electric conductivity ranging from 10 to 30%, due to induced defects as a result of alloying.[11] With surface modifications, the passive layer can undergo degradation at elevated temperatures attributed to the mismatch of the thermal expansion coefficient, thus exposing the metal underneath, causing its oxidation. The third strategy is to employ a dense oxide layer to passivate the conductor (e.g., atomic deposition of aluminum oxide (Al_2O_3)[11] or titanium dioxide (TiO_2)),[12–14] which can shield the conductor from oxidation and corrosion caused by atmospheric oxygen and corrosive environment at high temperatures. However, atomic deposition of thin oxide layers limits its throughput due to the long cycle times required for its chemical reactions contributing to massive material and energy waste.[15]

In contrast to conventional ceramics produced by solid state powder sintering, preceramic polymer-derived ceramics (PDCs) resulting from the thermal decomposition of liquid polymer precursors offer a versatile way to build ceramic composites with complex geometries, customized chemical compositions, and high mechanical flexibility to satisfy a wide range of applications.[16–19] Silicon oxide carbide (or silicon oxycarbide, SiOC) ceramics, one of the PDCs, are among the most promising matrix materials for high-temperature applications due to their superior antioxidation behavior and high-temperature anticreep performance.[20–22] Based on the thermal decomposition temperature, SiOC ceramics could be characterized as nanocomposites consisting of a silicon carbide (SiC_xO_y) matrix with free and turbostratic carbon.[23–25] Although the carbon-enriched SiOC matrix delivers minor conductivity (1×10^{-3} S cm^{-1}), it is far below the requirement of a functional conductor.[26]

Z. Li, S. Khuje, A. Islam, S. Ren
Department of Mechanical and Aerospace Engineering
University at Buffalo
The State University of New York
Buffalo, NY 14260, USA
E-mail: sren@umd.edu

Z. Li, S. Khuje, A. Islam, S. Ren
Department of Materials Science and Science
University of Maryland
College Park, MD 20742, USA

S. Ren
Department of Chemistry
University at Buffalo
The State University of New York
Buffalo, NY 14260, USA

S. Ren
Research and Education in Energy Environment & Water Institute
University at Buffalo
The State University of New York
Buffalo, NY 14260, USA

The ORCID identification number(s) for the author(s) of this article can be found under https://doi.org/10.1002/adem.202300957.

DOI: 10.1002/adem.202300957

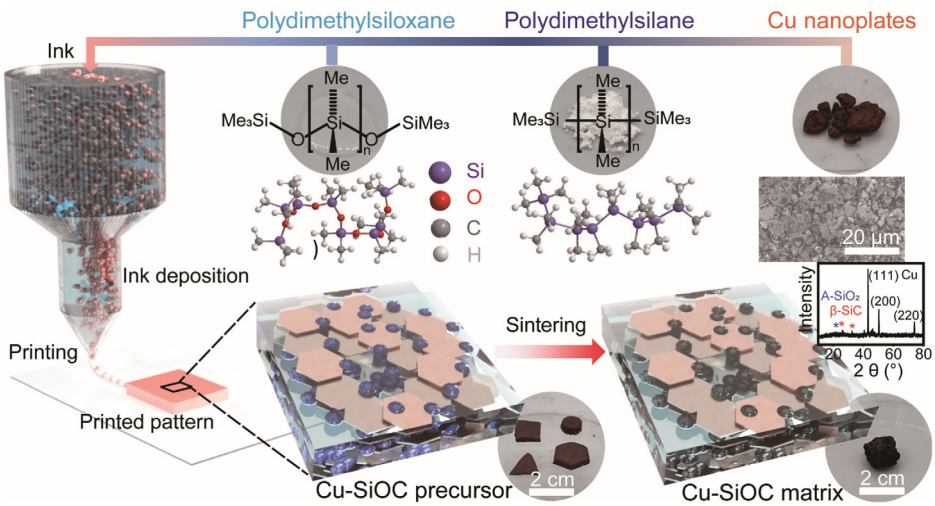

Figure 1. The schematic diagram of preceramic precursor-derived hybrid Cu and SiOC conductor for high-temperature stability, demonstrating the printing and sintering of Cu-based building blocks and additives.

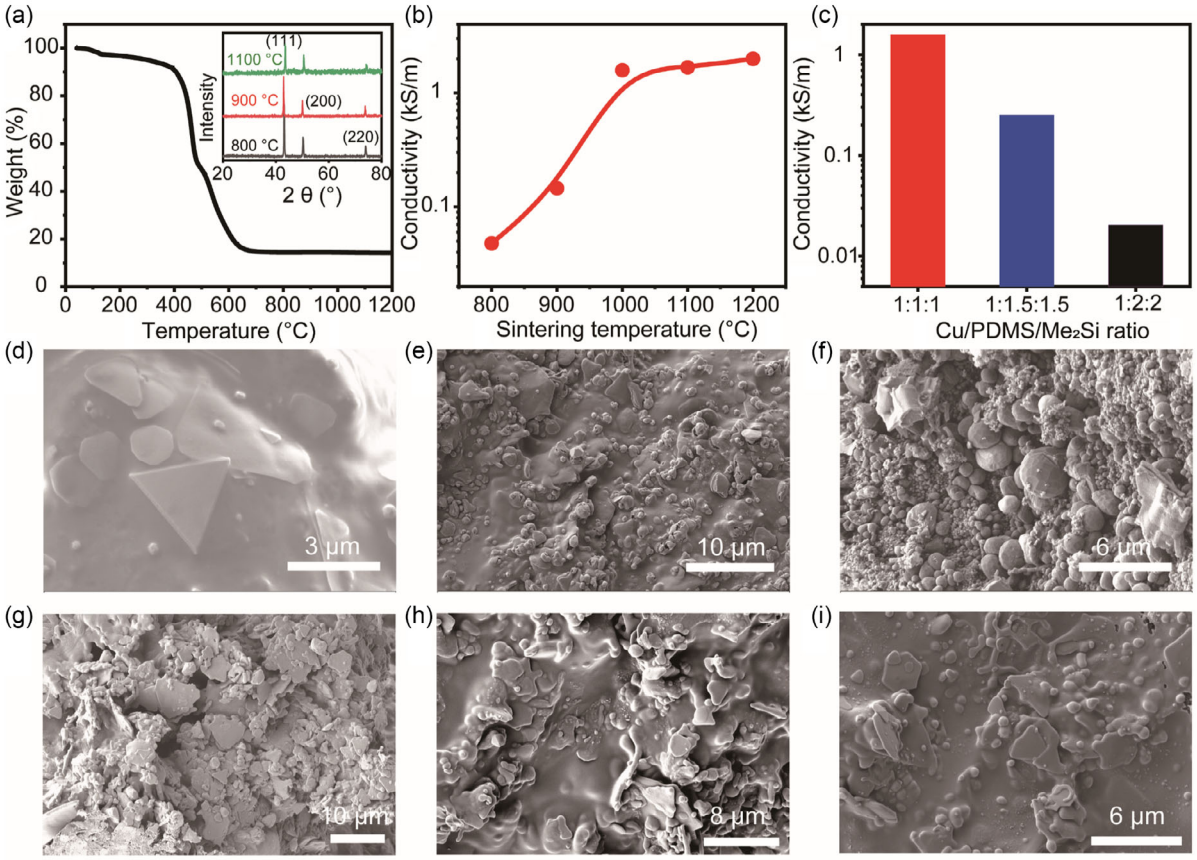

Figure 2. Structures and conductivity of Cu-incorporated SiOC ceramic conductor. a) TGA curve of the as-prepared Cu and SiOC precursor. Inset shows the XRD pattern of the as-prepared Cu and SiOC conductors under various sintering temperatures. b) Sintering temperature-dependent electrical conductivity of Cu and SiOC conductors. c) The corresponding conductivity of conductors with different Cu/PDMS/Me_2Si ratios. d) The SEM images of Cu–SiOC conductors before and after sintering e) under 1000 °C and f) 1200 °C. The SEM pictures of hybrid conductors after sintering with different Cu/PDMS/Me_2Si ratios: g) 1:1:1, h) 1:1.5:1.5, and i) 1:2:2.

Furthermore, SiOC oxidizes at ultrahigh temperatures due to the presence of free carbon in SiOC, affecting its thermal stability and electrical conductivity.[27] To overcome this challenge, new functional conductor materials based on SiOC systems capable of tolerating high temperatures are worth investigating. The metallic conductor copper (Cu), a commonly available conductive material employed in electronics, offers not only high electrical conductivity (58 MS m^{-1} at 20 °C) and a high melting point (1084 °C), but also noticeably plentiful and low cost.[28–30] Therefore, it would be interesting for incorporating Cu into the SiOC matrix, a potential candidate for high-temperature functional conductors.

2. Results and Discussion

Motivated by these considerations, we report additively manufacturing of high-temperature capable copper-reinforced SiOC conductor after pyrolysis of preceramic precursors,[31,32] enabling resistance temperature detectors (RTD) at high temperatures (**Figure 1**). The copper nanoplates (Cu NPLs) with 2D architecture are selected as the metallic building block. The polydimethylsiloxane (PDMS), polydimethylsilane (Me_2Si) and Cu NPLs are mixed to form a printable ink. Additive manufacturing offers a way to print 3D shapes. After the 3D-printed pattern is sintered, PDMS and Me_2Si convert to form SiOC and Cu NPLs and can maintain its high electrical and thermal conductivity. Moreover, the sintering procedure encourages the cross-woven architecture between Cu nanoplates and SiOC to enhance electrical conductivity and mechanical adhesion. SiOC acts as a high-temperature resistant material intimately wrapped around copper as a protective barrier to mitigate oxidation, while the copper framework provides effective electron channels throughout the material. Thus, the combination of these distinct advantages provides this composite material with excellent high-temperature resistance and superb structural thermal robustness under extreme conditions.

Figure 2a presents the thermogravimetric analysis (TGA) profiles of the ink material composed of Me_2Si, PDMS, and Cu NPLs. The ink decomposition starts at 390 °C and continues until 700 °C when the ink decomposes completely and the mass changes to ≈17% of the initial weight.[33] The TGA curves corresponding to polymethylsiloxanes and polydimethylsilane have been previously reported.[33,34] The inset shows the X-ray diffraction (XRD) pattern of the as-prepared Cu and SiOC composites under various sintering temperatures, where the 2θ peaks emerge at 43.3°, 50.5°, and 74.1° associated with the {111}, {200}, and {220} Cu planes. Post-sintering processing of the printed patterns is essential to improve the electrical conductivity while inducing the conversion of polydimethylsiloxane and polydimethylsilane precursors to SiOC, thus enhancing the contact between SiOC and Cu NPLs and density of Cu and SiOC matrix. By altering the sintering temperature, the electrical conductivity

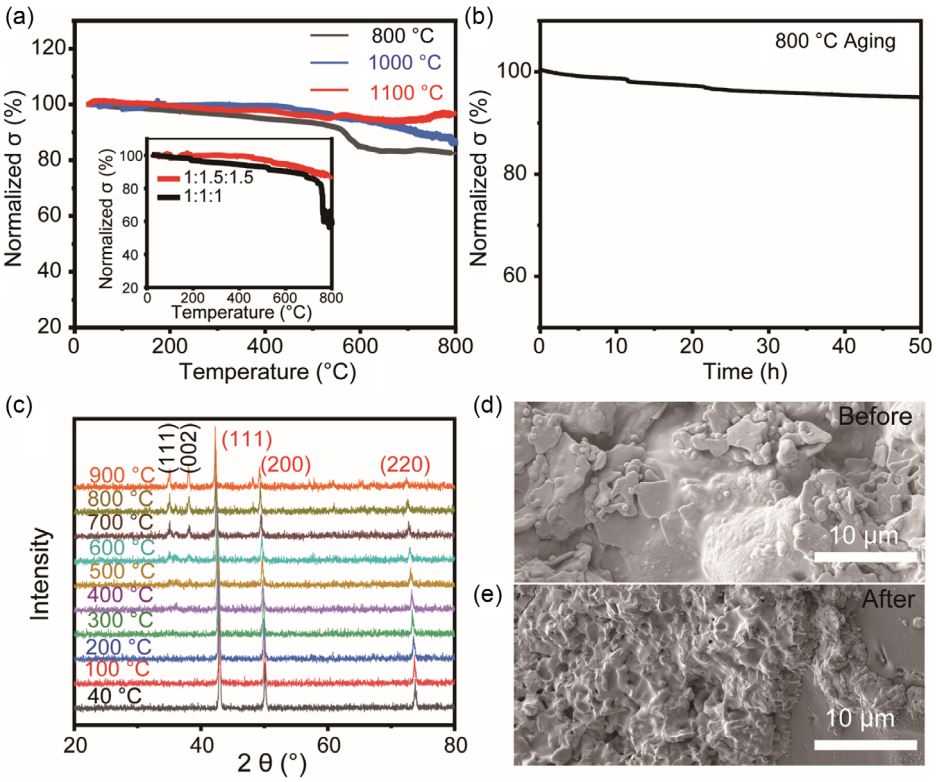

Figure 3. High-temperature performance of hybrid Cu and SiOC ceramic conductor. a) The normalized conductivity versus temperature curve of as-prepared Cu and SiOC ceramic conductor sintering under various temperatures. Inset shows the temperature-dependent normalized conductivity of Cu and SiOC conductor with different Cu/PDMS/Me_2Si ratio. b) Diagram plotting the normalized conductivity as a function of time, revealing the stability of the Cu and SiOC conductor at 800 °C. c) In situ XRD spectra of Cu–SiOC conductor measured at different temperatures from 40 to 900 °C and ambient environmental conditions. SEM images representing the Cu and SiOC ceramic conductor before d) and after e) tested at 900 °C.

of Cu and SiOC composite dramatically increases from 0.045 kS m^{-1} at 800 °C to 1.1 kS m^{-1} at 1200 °C (Figure 2b). It is evident that the electric conductivity of the Cu-SiOC complex is significantly superior to that of the carbon-rich SiOC matrix. Furthermore, the greatest rise of electrical conductivity was observed at sintering temperatures from 800 to 1000 °C. Figure 2d–f and S1, Supporting Information, reveal the scanning electron microscope (SEM) images of Cu and SiOC conductors before and after sintering under various temperatures. From the SEM image, the Cu NPLs are melted from the composites annealed under 1200 °C. Figure 2c demonstrates the electrical conductivity of the Cu and SiOC features as a function of Cu/PDMS/Me_2Si ratio. When the Cu/PDMS/Me_2Si ratio is 1:1:1, the conductivity of sintered Cu and SiOC conductor achieves 1.06 kS m^{-1}. As the Cu/PDMS/Me_2Si ratio changes to 1:2:2, the conductivity of Cu and SiOC conductor decreases to 0.02 kS m^{-1}. The SEM images with different Cu/PDMS/Me_2Si ratios displayed in Figure 2g–i, illustrating that the ratio of Cu in the composites, decrease with increasing PDMS and Me_2Si content, which is consistent with the conductivity with different Cu/PDMS/Me_2Si ratios, indicating that the conductivity of the complex is mainly contributed by Cu NPLs.

To investigate the resistance to oxidation of Cu and SiOC conductors, we varied the sintering temperature and the weight percentage of PDMS and Me_2Si of the Cu and SiOC composites to evaluate their impact on high-temperature-dependent conductivity and stability in atmosphere environment (**Figure 3**a). In comparison, the Cu and SiOC composites sintered under 1000 and 1100 °C show the temperature stability withstanding at 800 °C. The inset shows the increased tolerance temperature of 800 °C when the ratio of Cu/PDMS/Me_2Si changes from 1:1:1 to 1:1.5:1.5. Therefore, the Cu/SiOC composite prepared under 1000 °C sintering temperature and ratio of Cu/PDMS/Me_2Si with 1:1.5:1.5 was selected as a prototype case for carrying out further experiments. Figure 3b exhibits the resistance of the Cu and SiOC conductor at 800 °C. It can be clearly observed that the conductivity stays above 90% of the initial conductivity after about 50 h of aging, indicating that Cu and SiOC can implement prolonged reliability at 800 °C. Cu-SiOC and silicon oxycarbide composite[35] demonstrates similar ultrahigh oxidation resistance characteristics under oxygen conditions. However, Cu-SiOC exhibits superior elevated temperature oxidation-resistant and thermal stability compared with Cu alloy (e.g., CuAg, CuCr, CuPa, CuMg)[36,37] and Cu–graphene complexes.[11]

Figure 3c demonstrates the XRD patterns of the Cu and SiOC conductor in situ tested at different temperature conditions from 40 to 900 °C. When the temperature rises to 600 °C, new peaks appear at 35.55° and 38.41°, corresponding to CuO planes of {002} and {111}. The corresponding SEM images before and after tested at 900 °C are shown in Figure 3d–e, suggesting that the surface Cu is oxidized while the Cu impregnated into the SiOC matrix is intact.

The hybrid Cu and SiOC conductor provides significant resistance under high-temperature conditions, allowing it to be an outstanding candidate material for temperature sensing, that is, RTD. **Figure 4**a presents the resistance variation of the conductor under the hydrogen torch test. The resistance also

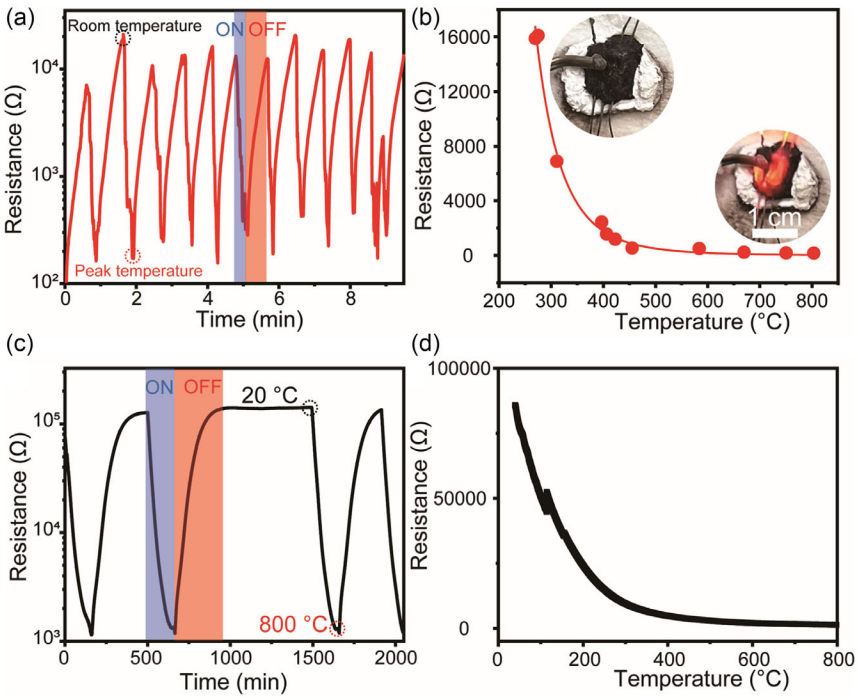

Figure 4. High-temperature resistance temperature sensing of Cu and SiOC ceramic conductor. a) The on–off cycle testing of Cu and SiOC ceramic conductors under hydrogen torch test. b) Plot depicting the resistance-dependent temperature of Cu and SiOC ceramic conductor with linear fitting curve for RTD sensor exposed to hydrogen torch test. c) Resistance as a function of heating and cooling cycles for Cu and SiOC conductor under furnace heating with the heating rate of 5 °C min^{-1} and air cooling. d) Plot depicting the resistance-dependent temperature of Cu and SiOC ceramic conductor with linear fitting curve using furnace air cooling.

varies dramatically during the heating-up and cooling-down (ON–OFF) process and displays excellent repeatability. The resistance versus temperature profile of Cu and SiOC conductor depicted in Figure 4b shows a negative temperature coefficient of resistance (TCR) under ambient conditions, while its conductivity increases with elevated temperature as more carriers are available because of thermal motion. Figure 4c shows the steady-state heating and cooling ON–OFF curve from 20 to 800 °C with a 5 °C min^{-1} temperature increase and air-cooling rate. The results are consistent with the hydrogen torch, with high-level stability and reliability. The temperature-dependent resistance can be established by fitting a profile to the Cu and SiOC conductor via applying a polynomial equation (Figure 4b, d): $R_T = R_0 + A * T + B * T^2 + C * T^3 + D * T^4 + E * T^5$, where R_0 and R_T respectively represent the initial resistance and the resistance at temperature T. According to the hydrogen torch test data, $R_0 = 467\,997$, $A = -4190$, $B = 14.85$, $C = -0.02$, $D = 2.22 \times 10^{-5}$, $E = -7.53 \times 10^{-9}$, and for the steady-state test, $R_0 = 105\,080$, $A = -649$, $B = 1.47$, $C = -0.001$, $D = -4.61 \times 10^{-8}$, $E = 3.85 \times 10^{-10}$. The Cu and SiOC ceramics with high melting point and robustness offer an option for high-temperature electronics.

3. Conclusion

In summary, we reported a printable metal-reinforced ceramic composite material consisting of preceramic-derived SiOC and copper with electrical resistance and durability at high temperatures through additive manufacturing. The SiOC is prepared by in situ conversion of Me_2Si and PDMS and maintains high-temperature stability beyond 800 °C. The as-prepared hybrid conductors exhibit negative TCR coefficient and stay constant after consecutive high-temperature tests with remarkable repeatability, indicating that the synergistic effect of copper integration into SiOC not only boosts the electrical conductivity of the system but also preserves its antioxidation reliability. This approach opens up the possibility of producing printed conductors with scalable manufacturing and high-temperature tolerance by combining metal or highly conductive materials with SiOC, which offer the route to electronic products for high-temperature usage purposes under harsh environment.

4. Experimental Section

The Synthesis of Dried Cu NPLs Powder: First, 2.4 g copper chloride dihydrate ($CuCl_2{\cdot}2H_2O$), 3.9 g D-glucose ($C_6H_{12}O_6$), 14.55 g hexadecylamine (HDA), and 90 mg sodium iodide (NaI) were dispersed into 900 mL of deionized (DI) water by stirring overnight until a homogeneous emulsion was achieved. Then, the mixed solution was placed in a hydrothermal reactor and heated for a duration of 12 h at 100 °C. The Cu NPLs dispersed in the solution were gathered by centrifugation at 5000 rpm for 5 min. The gained solids were redispersed in DI water and the centrifugation process was repeated to remove impurities. The Cu NPLs were once again dispersed into ionized water and ethanol mixture (weight ratio of DI water: ethanol = 1:1) for further cleaning. Finally, dried Cu NPLs powder was obtained by dry Cu NPLs feedstock in vacuum oven.

The Preparation of Cu-SiOC Conductors: Dried Cu NPLs, polydimethylsiloxane (PDMS), and poly(dimethylsilane) (PDS) were mixed via ARE-310 Thinky Mixer with 2000 rpm for 7 min to obtain the printable Cu–SiOC ink. The printed pattern on alumina ribbon ceramic substrate was sintered under forming gas (5% H_2% and 95% N_2) and at different temperatures (800–1200 °C) to prepare Cu–SiOC conductors.

Hydrogen Torch Test: The Cu–SiOC sample was first glued to the silica aerogel substrate with Ultra-Temp 516 ceramic glue. A Keithley 2450 Sourcemeter and K-type thermocouple were used to monitor and record resistance and temperature. The temperature of the sample was varied by controlling the distance between the torch generated by hydrogen generator and the sample.

Morphological and Structural Characterizations: The Carl Zeiss AURIGA crossbeam focused ion beam–SEM (FIB–SEM) was used to acquire SEM pictures. TGA data was obtained from the SDT Q600 thermogravimetric analyzer under N_2. Rigaku Ultima IV instrument was utilized to collect XRD patterns. The electrical properties were captured by a Keithley 2450 Sourcemeter.

Supporting Information

Supporting Information is available from the Wiley Online Library or from the author.

Acknowledgements

Financial support was provided by the U.S. Army Research Laboratory Support S. R. under award W911NF-20-2-0016.

Conflict of Interest

The authors declare no conflict of interest.

Author Contributions

Z.L. carried out all the experiments. S.K. performed the hydrogen torch test. A.I. helped to provide the schematic figure. S. R. designed the experiment. All authors commented on the final manuscript.

Data Availability Statement

The data that support the findings of this study are available from the corresponding author upon reasonable request.

Keywords

additive manufacturing, copper, high temperatures, preceramic materials, silicon oxycarbides

Received: June 23, 2023
Revised: August 7, 2023
Published online: September 28, 2023

[1] J. Watson, G. Castro, *J. Mater. Sci.: Mater. Electron.* **2015**, *26*, 9226.
[2] A. Sheng, S. Khuje, J. Yu, C.-G. Zhuang, S. Ren, *Adv. Eng. Mater.* **2022**, *25*, 2201056.
[3] E. Bagheri, L. Ansari, E. Sameiyan, K. Abnous, S. M. Taghdisi, M. Ramezani, M. Alibolandi, *Biosens. Bioelectron.* **2020**, *153*, 112054.
[4] S. Naghdi, K. Y. Rhee, D. Hui, S. Park, *Coatings* **2018**, *8*, 278.
[5] M. Eto, N. Araki, T. Yamada, M. Sugiyama, S. Fujimoto, *Microelectron. Reliab.* **2021**, *120*, 114125.
[6] I. Janowska, M.-S. Moldovan, O. Ersen, H. Bulou, K. Chizari, M. J. Ledoux, C. Pham-Huu, *Nano Res.* **2011**, *4*, 511.

[7] A. Sheng, S. Khuje, J. Yu, D. Petit, T. Parker, C. G. Zhuang, L. Kester, S. Ren, *Nano Lett.* **2021**, *21*, 9279.
[8] C. Yim, Z. A. Kockerbeck, S. B. Jo, S. S. Park, *ACS Appl. Mater. Interfaces* **2017**, *9*, 37160.
[9] S. Chen, L. Brown, M. Levendorf, W. Cai, S. Y. Ju, J. Edgeworth, X. Li, C. W. Magnuson, A. Velamakanni, R. D. Piner, J. Kang, J. Park, R. S. Ruoff, *ACS Nano* **2011**, *5*, 1321.
[10] G. Liu, J. Wang, Y. Ge, Y. Wang, S. Lu, Y. Zhao, Y. Tang, A. M. Soomro, Q. Hong, X. Yang, F. Xu, S. Li, L. J. Chen, D. Cai, J. Kang, *ACS Nano* **2020**, *14*, 6761.
[11] S. Khuje, F. Alshatnawi, M. Alhendi, J. Yu, A. Sheng, Y. Huang, C. G. Zhuang, J. Armstrong, C. Zhou, M. Poliks, S. Ren, *Adv. Electron. Mater.* **2022**, *9*, 2200979.
[12] J. S. Daubert, G. T. Hill, H. N. Gotsch, A. P. Gremaud, J. S. Ovental, P. S. Williams, C. J. Oldham, G. N. Parsons, *ACS Appl. Mater. Interfaces* **2017**, *9*, 4192.
[13] V. Dias, H. Maciel, M. Fraga, A. O. Lobo, R. Pessoa, F. R. Marciano, *Materials* **2019**, *12*, 682.
[14] A. I. Abdulagatov, Y. Yan, J. R. Cooper, Y. Zhang, Z. M. Gibbs, A. S. Cavanagh, R. G. Yang, Y. C. Lee, S. M. George, *ACS Appl. Mater. Interfaces* **2011**, *3*, 4593.
[15] P. O. Oviroh, R. Akbarzadeh, D. Pan, R. A. M. Coetzee, T. C. Jen, *Sci. Technol. Adv. Mater.* **2019**, *20*, 465.
[16] Y. Jia, T. D. Ajayi, J. Morales, M. A. R. Chowdhury, G. Sauti, S. H. Chu, C. Park, C. Xu, *J. Am. Ceram. Soc.* **2019**, *102*, 7584.
[17] J. Yang, J. Sprengard, L. Ju, A. Hao, M. Saei, R. Liang, G. J. Cheng, C. Xu, *Carbon* **2016**, *108*, 38.
[18] Z. Ren, S. B. Mujib, G. Singh, *Materials* **2021**, *14*, 614.
[19] R. P. Chaudhary, C. Parameswaran, M. Idrees, A. S. Rasaki, C. Liu, Z. Chen, P. Colombo, *Prog. Mater Sci.* **2022**, *128*, 100969.
[20] Y. Jia, T. D. Ajayi, M. A. Roberts Jr., C. C. Chung, C. Xu, *ACS Appl. Mater. Interfaces* **2020**, *12*, 46254.
[21] C. Stabler, A. Reitz, P. Stein, B. Albert, R. Riedel, E. Ionescu, *Materials* **2018**, *11*, 279.
[22] J. Sun, T. Li, A. Reitz, Q. Fu, R. Riedel, Z. Yu, *Corros. Sci.* **2020**, *175*, 108866.
[23] K. Lu, D. Erb, M. Liu, *J. Mater. Chem. C* **2016**, *4*, 1829.
[24] J. Li, K. Lu, R. Riedel, *J. Am. Ceram. Soc.* **2015**, *98*, 2357.
[25] A. Saha, R. Raj, *J. Am. Ceram. Soc.* **2007**, *90*, 578.
[26] K. Wang, B. Ma, X. Li, Y. Wang, L. An, R. Riedel, *J. Am. Ceram. Soc.* **2014**, *97*, 2135.
[27] F. Kolář, V. Machovič, J. Svítilová, L. Borecká, *Mater. Chem. Phys.* **2004**, *86*, 88.
[28] Z. Li, S. Khuje, A. Chivate, Y. Huang, Y. Hu, L. An, Z. Shao, J. Wang, S. Chang, S. Ren, *ACS Appl. Electron. Mater.* **2020**, *2*, 1867.
[29] J. W. Lee, J. Han, D. S. Lee, S. Bae, S. H. Lee, S. K. Lee, B. J. Moon, C. J. Choi, G. Wang, T. W. Kim, *Small* **2018**, *14*, 1703312.
[30] C. Subramaniam, T. Yamada, K. Kobashi, A. Sekiguchi, D. N. Futaba, M. Yumura, K. Hata, *Nat. Commun.* **2013**, *4*, 2202.
[31] J. Bauer, C. Crook, T. Baldacchini, *Science* **2023**, *380*, 960.
[32] H. Dory, P. Miele, C. Salameh, *Int. J. Appl. Ceram. Technol.* **2022**, *20*, 141.
[33] N. K. Sethy, Z. Arif, P. K. Mishra, P. Kumar, *J. Polym. Eng.* **2019**, *39*, 679.
[34] H. Okumura, Y. Kawaguchi, A. Harada, *Macromolecules* **2003**, *36*, 6422.
[35] T. Xu, Q. Ma, Z. Chen, *Ceram. Int.* **2011**, *37*, 2555.
[36] P. J. Ding, W. A. Lanford, S. Hymes, S. P. Murarka, *Appl. Phys. Lett.* **1994**, *64*, 2897.
[37] L. Ogbuji, D. L. Humphrey, *Oxid. Met.* **2003**, *60*, 271.